Article

Cell Metabolism

Dysfunction of Natural Killer Cells by FBP1-Induced Inhibition of Glycolysis during Lung Cancer Progression

Graphical Abstract

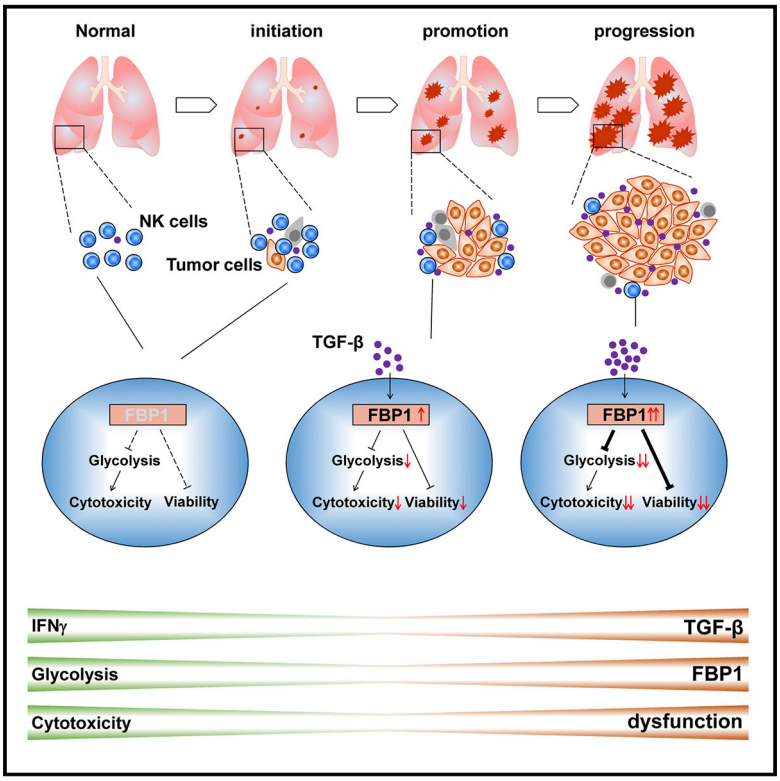

Highlights

- NK cells prevent tumor initiation but do not control tumor promotion or progression
- FBP1 elicits dysfunction of NK cells by impairing glycolysis and viability
- FBP1 inhibition restores the function of NK cells

Authors

Jingjing Cong, Xianwei Wang, Xiaohu Zheng, ..., Rui Sun, Zhigang Tian, Haiming Wei

Correspondence

tzg@ustc.edu.cn (Z.T.), ustcwhm@ustc.edu.cn (H.W.)

In Brief

Cong et al. demonstrate that NK cells lose their antitumor effect gradually and ultimately evolve into a dysfunctional state during tumor development. The tumor microenvironment disables NK cells by weakening their glycolytic metabolism, thus promoting tumor immune escape; remarkably, FBP1 acts as a key molecule in this process.

Cong et al., 2018, Cell Metabolism *28*, 243–255
August 7, 2018
https://doi.org/10.1016/j.cmet.2018.06.021

CellPress

Cell Metabolism
Article

Dysfunction of Natural Killer Cells by FBP1-Induced Inhibition of Glycolysis during Lung Cancer Progression

Jingjing Cong,[1] Xianwei Wang,[1] Xiaohu Zheng,[1] Dong Wang,[1] Binqing Fu,[1,2] Rui Sun,[1,2] Zhigang Tian,[1,2,*] and Haiming Wei[1,2,3,*]

[1]The CAS Key Laboratory of Innate Immunity and Chronic Disease and Institute of Immunology, School of Life Science and Medical Center, University of Science and Technology of China, Hefei, Anhui 230027, China

[2]Hefei National Laboratory for Physical Sciences at Microscale, University of Science and Technology of China, Hefei, Anhui 230027, China

[3]Lead Contact

*Correspondence: tzg@ustc.edu.cn (Z.T.), ustcwhm@ustc.edu.cn (H.W.)

https://doi.org/10.1016/j.cmet.2018.06.021

SUMMARY

Natural killer (NK) cells are effector lymphocytes with pivotal roles in the resistance against various tumors; dysfunction of NK cells often results in advanced tumor progression. Tumors develop in three stages comprising initiation, promotion, and progression, but little is known about the interrelationships between NK cells and tumor cells at different stages of tumor development. Here, we demonstrated that NK cells prevented tumor initiation potently but did not prevent tumor promotion or tumor progression in *Kras*-driven lung cancer. Moreover, loss of the antitumor effect in NK cells was closely associated with their dysfunctional state during tumor promotion and progression. Mechanistically, aberrant fructose-1,6-bisphosphatase (FBP1) expression in NK cells elicited their dysfunction by inhibiting glycolysis and impairing viability. Thus, our results show dynamic alterations of NK cells during tumor development and uncover a novel mechanism involved in NK cell dysfunction, suggesting potential directions for NK cell-based cancer immunotherapy involving FBP1 targeting.

INTRODUCTION

Lung cancer has very high mortality rates worldwide, and ≈80% of lung cancer is classified as non-small cell lung cancer (NSCLC) (Reck et al., 2013; Siegel et al., 2012). NSCLC is classified further into adenocarcinoma (≈50%), squamous cell carcinoma (≈40%), and large cell carcinoma (≈10%) according to its pathologic characteristics (Chen et al., 2014). *KRAS* mutations, found in ≈30% of adenocarcinomas, are the most common mutations, but targeted therapies for NSCLC patients with *KRAS* mutations are lacking (Chen et al., 2014; Roberts and Stinchcombe, 2013). Recently, immunotherapy, represented by blockade of the PD1-PDL1 checkpoint, has been reported as being efficient in patients with various types of advanced cancers, including NSCLC (Brahmer et al., 2012; Topalian et al., 2012). Moreover, infiltrating immune cells in human tumors have a significant effect on the prognosis and therapies (Fridman et al., 2012). Therefore, focusing on the immune microenvironment and investigating potential immunotherapies could contribute to controlling *KRAS*-driven lung cancer.

Natural killer (NK) cells are cytotoxic innate immune cells with established roles in resisting numerous tumor types (Malmberg et al., 2017; Vivier et al., 2008). NK cells eliminate tumor cells by various mechanisms, including granules (perforin/granzyme) exocytosis, death receptors (FAS-FASL, TRAIL-TRAILR), and secretion of effector molecules (interferon-γ [IFN-γ], tumor necrosis factor α [TNF-α], NO) (Smyth et al., 2002). However, tumor cells evade NK cell-mediated surveillance by developing an immunosuppressive microenvironment in which NK cell dysfunction is caused by direct crosstalk between tumor cells and NK cells, activated platelets and several soluble factors, such as myeloid-derived suppressor cells (MDSCs), and macrophage- and tumor cell-derived transforming growth factor β (TGF-β), prostaglandin E_2, indoleamine-2,3-dioxygenase, adenosine, and interleukin-10 (IL-10) (Morvan and Lanier, 2016). In addition, once a tumor is entrenched, NK cells cannot infiltrate intratumoral areas readily, and intratumoral NK cells exhibit altered phenotypes and functions relative to non-tumoral NK cells in patients with lung cancer (Carrega et al., 2008; Platonova et al., 2011), prostate cancer (Pasero et al., 2016), breast cancer (Mamessier et al., 2011), hepatocellular carcinoma (Xu et al., 2017; Zhang et al., 2017), and gastrointestinal stromal tumors (Rusakiewicz et al., 2013).

NK cells comprise 10%–20% of lymphocytes in the lungs of humans and mice, and the vast majority of NK cells have a mature phenotype. In homeostasis, NK cells in the human lung are in a hypofunctional state compared with NK cells in peripheral blood and the spleen (Bjorkstrom et al., 2016; Gregoire et al., 2007; Robinson et al., 1984). Similarly, compared with NK cells in the spleen and bone marrow, NK cells in the mouse lung are subject to tighter restrictions under normal conditions and need to overcome a higher threshold of inhibition to become activated (Culley, 2009; Wang et al., 2012). Recent studies have reported that in NSCLC patients, intratumoral NK cells have a reduced number, decreased expression of NK cell receptors, defective degranulation and IFN-γ production, and a proangiogenic phenotype relative to non-tumoral NK cells (Bruno et al.,

2013; Lavin et al., 2017; Platonova et al., 2011). However, very little is known about the role of NK cells in lung cancer development, especially in *KRAS*-driven lung cancer. Moreover, the functional states, distribution, phenotypes, and regulation of NK cells in the microenvironment of *KRAS*-driven lung cancer have not been reported.

Increasingly, it is accepted that cellular metabolism is important for immune function and that metabolic changes can dominate immune responses directly (Biswas, 2015; Gardiner and Finlay, 2017; O'Neill et al., 2016). Considerable attention has been focused on T cells and macrophages (Biswas, 2015; Kishton et al., 2017; Wenes et al., 2016; Zhao et al., 2016), and little is known about NK cell metabolism. In humans, increased glycolysis and oxidative phosphorylation (OXPHOS) support IFN-γ production by $CD56^{bright}$ NK cells (Keating et al., 2016). In mice, steady-state NK cells favor OXPHOS, rather than glycolysis, as the primary metabolic pathway, whereas IL-2/IL-12-induced activated NK cells have a greater tendency to use glycolysis for rapid biosynthetic purposes. In addition, direct inhibition of glycolysis weakens the effector functions of NK cells (Donnelly et al., 2014; Keppel et al., 2015). Thus, glycolysis is important for NK cell function, and there is, in general, improved glycolysis in activated NK cells. However, changes in glycolysis and the correlations between glycolytic changes and effector functions of NK cells in cancer are not known.

Fructose-1,6-bisphosphatase (FBP1), a rate-limiting enzyme involved in gluconeogenesis, mainly facilitates gluconeogenesis and inhibits glycolysis. Deficiency of FBP1 is associated with lactic acidosis and hypoglycemia, which can lead to unexpected death in infants (Emery et al., 1988). In addition to its roles in glucose metabolism, *in vitro* genetic manipulation experiments have shown that FBP1 can restrain cell growth and induce reactive oxygen species (ROS) production (Chen et al., 2011; Dong et al., 2013; Li et al., 2014). FBP1 has been reported to have a tumor-suppressive role in certain tumor types; accordingly, loss of FBP1 promotes tumor progression by enhancing glycolysis and restraining cell growth, thereby leading to a poor prognosis in patients with breast cancer, renal cell carcinoma, and hepatocellular carcinoma (Dong et al., 2013; Hirata et al., 2016; Li et al., 2014). However, expression of FBP1 in immune cells and whether aberrant expression of FBP1 influences immune cell metabolism have not been investigated.

Here, we comprehensively studied NK cells from tumor initiation to tumor promotion and, ultimately, to tumor progression in a *Kras*-driven model of spontaneous lung cancer. We provide evidence that NK cells were gradually induced into a dysfunctional state and increasingly lost their antitumor effect during lung cancer development. Furthermore, NK cell dysfunction was elicited by FBP1-mediated inhibition of glycolysis and impaired viability. Our results reveal a novel mechanism involved in NK cell dysfunction and suggest that targeting FBP1 could be a promising approach for restoring functions of NK cells during lung cancer treatment.

RESULTS

NK Cells Prevent Lung Cancer Initiation

To investigate the role of NK cells throughout all stages of lung cancer development, we used a Cre-inducible $Kras^{G12D}$ (*Kras*) knockin mouse lung cancer model. In this model, tumor development can be evaluated using a three-stage system (DuPage et al., 2009). At 4–6 weeks after pCDH-CMV-MCS-EF1-Cre (Lenti-Cre) delivery (stage 1), mutant *Kras* transformed lung epithelial cells, and atypical adenomatous hyperplasia or small adenomas were observed as the earliest lesions. At 8–13 weeks after Lenti-Cre delivery (stage 2), transformed cells underwent benign proliferation, and larger adenomas with uniform nuclei were evident. At 15 weeks after Lenti-Cre delivery (stage 3), which was a malignant phase, typical adenocarcinomas with pleomorphic nuclei began to appear (Figure 1A). These three stages closely recapitulated the three main phases of carcinogenesis: initiation (acquiring mutations), promotion (benign proliferation), and progression (malignant transformation). The lung weight increased gradually, but body weight and spleen weight remained unchanged as lung cancer developed (Figure 1B).

Based on information regarding the timing of lung carcinogenesis, we used anti-NK1.1 mAb-PK136 to deplete the number of NK cells during tumor initiation, or tumor promotion and progression, to determine the role of NK cells at different stages of lung cancer. Administration of PK136 decreased the number of lung NK cells in *Kras* mice significantly (Figures 1E and 1H). Strikingly, depletion of NK cells during tumor initiation accelerated tumor development significantly (Figures 1C and 1D), whereas depletion of NK cells during tumor promotion and tumor progression did not affect tumor development (Figures 1F and 1G). To confirm these observations, we crossed *Kras* mice with $Nfil3^{-/-}$ mice (which are devoid of NK cells) to produce *Kras*;$Nfil3^{-/-}$ mice, which could develop *Kras*-driven lung cancer spontaneously, with a concomitant lack of NK cells (Figure 1K). At 10 weeks after Lenti-Cre delivery, *Kras*;$Nfil3^{-/-}$ mice developed more severe lung cancer compared with *Kras* mice (Figures 1I and 1J). Consistent with the *Kras* model, in the mouse Lewis lung carcinoma (LLC) lung metastasis model, more and larger tumor nodules were observed in the lungs of $Nfil3^{-/-}$ mice compared with wild-type (WT) mice (Figures 1L and 1M). The lack of NK cells in the lungs of $Nfil3^{-/-}$ mice was demonstrated by flow cytometry (FCM) (Figure 1N). Taken together, these findings show that NK cells prevent tumor initiation potently but fail to control the promotion and progression of lung cancer.

NK Cells Clearly Decrease in Number during Lung Cancer Progression

Given the finding that the antitumor effect of NK cells alters according to the stage of lung cancer, we undertook in-depth research into NK cells by lung cancer stage. We hypothesized that loss of the antitumor effect by NK cells could be caused by their decreased number and effector functions during lung cancer promotion and progression. Accordingly, we quantified and localized NK cells during lung cancer development. FCM was used to analyze leukocytes isolated from the lungs and spleens of WT and *Kras* mice at different stages of lung cancer (Figure 2A). The frequency and number of NK cells, T cells, B cells, and MDSCs in the lungs showed a progressive decline, whereas macrophages showed the opposite trend (Figures 2B–2D). Conversely, the composition of spleen leukocytes remained constant (Figure S1). Notably, the loss of NK cells in the lungs was the most pronounced (from 9.3% to 2.3%, a 4-fold

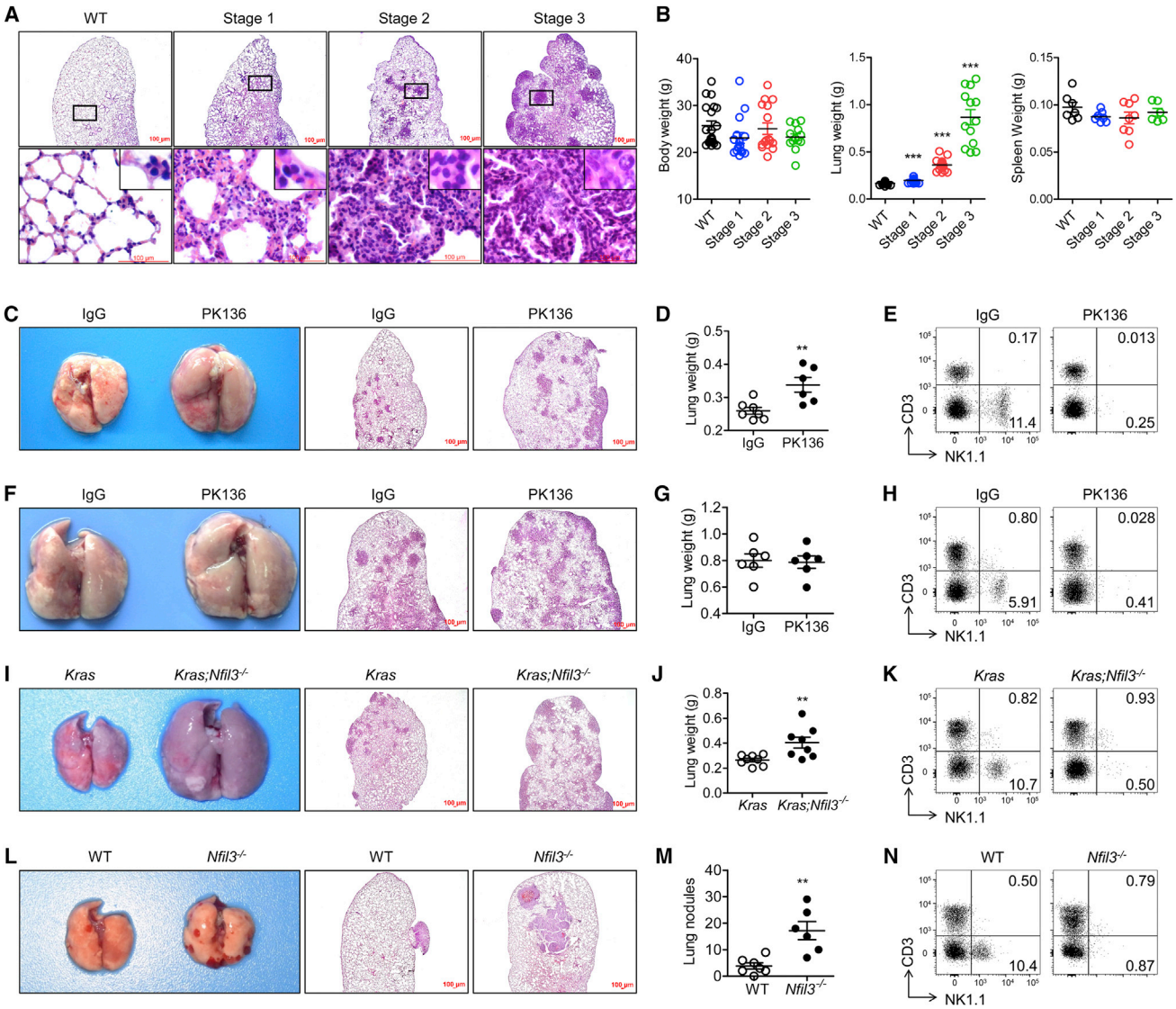

Figure 1. NK Cells Potently Prevent Tumor Initiation, but Fail to Control the Promotion and Progression of Lung Cancer

(A) Representative histology of the H&E-stained lungs of wild-type (WT) mice and lesions in the lungs of *Kras* mice at different stages of lung cancer. Results are representative of three independent experiments.

(B) Body weight, lung weight, and spleen weight of WT mice and *Kras* mice; n = 13–21 for body weight and lung weight groups; n = 6–7 for the spleen weight group. Data are pooled from seven independent experiments.

(C–E) *Kras* mice were infected (intranasally) with Lenti-Cre followed by administration of PK136 or immunoglobulin G (IgG) every week. Mice were sacrificed 10 weeks after Lenti-Cre infection. Representative appearance and histology of lungs (C), lung weight (D), and representative FCM plots of NK cells (E) in the lungs are shown; n = 6–7.

(F–H) *Kras* mice were infected (intranasally) with Lenti-Cre followed by administration of PK136 or IgG every week from week 10. Mice were sacrificed 15 weeks after Lenti-Cre infection. Representative appearance and histology of lungs (F), lung weight (G), and representative FCM plots of NK cells (H) in the lungs are shown; n = 6.

(I–K) *Kras* and *Kras;Nfil3*$^{-/-}$ mice were infected (intranasally) with Lenti-Cre. Mice were sacrificed 10 weeks after Lenti-Cre infection. Representative appearance and histology of lungs (I), lung weight (J), and representative FCM plots of NK cells (K) in the lungs are shown; n = 8.

(L–N) WT and *Nfil3*$^{-/-}$ mice were injected (intravenously) with LLC cells. Mice were sacrificed 15 days after injection. Representative appearance and histology of lungs (L), the number of tumor nodules (M), and representative FCM plots of NK cells (N) in the lungs are shown; n = 6–7.

Scale bars, 100 μm (A, C, F, I, and L). Each symbol in (B), (D), (G), (J), and (M) represents an individual mouse. Data are presented as mean ± SEM. Unpaired t test, $^{**}p < 0.01$ and $^{***}p < 0.001$.

decrease; with a reduction from 2.6 × 10^6/g to 0.42 × 10^6/g, a 6-fold decrease), with a particularly sharp decline at stage 2 (Figures 2B–2D). To determine the tissue localization of NK cells, we carried out immunofluorescence using an NK1.1 marker. NK cells were located mainly adjacent to the tumor, with rare infiltration into tumor lesions (Figure 2E). These results show that the

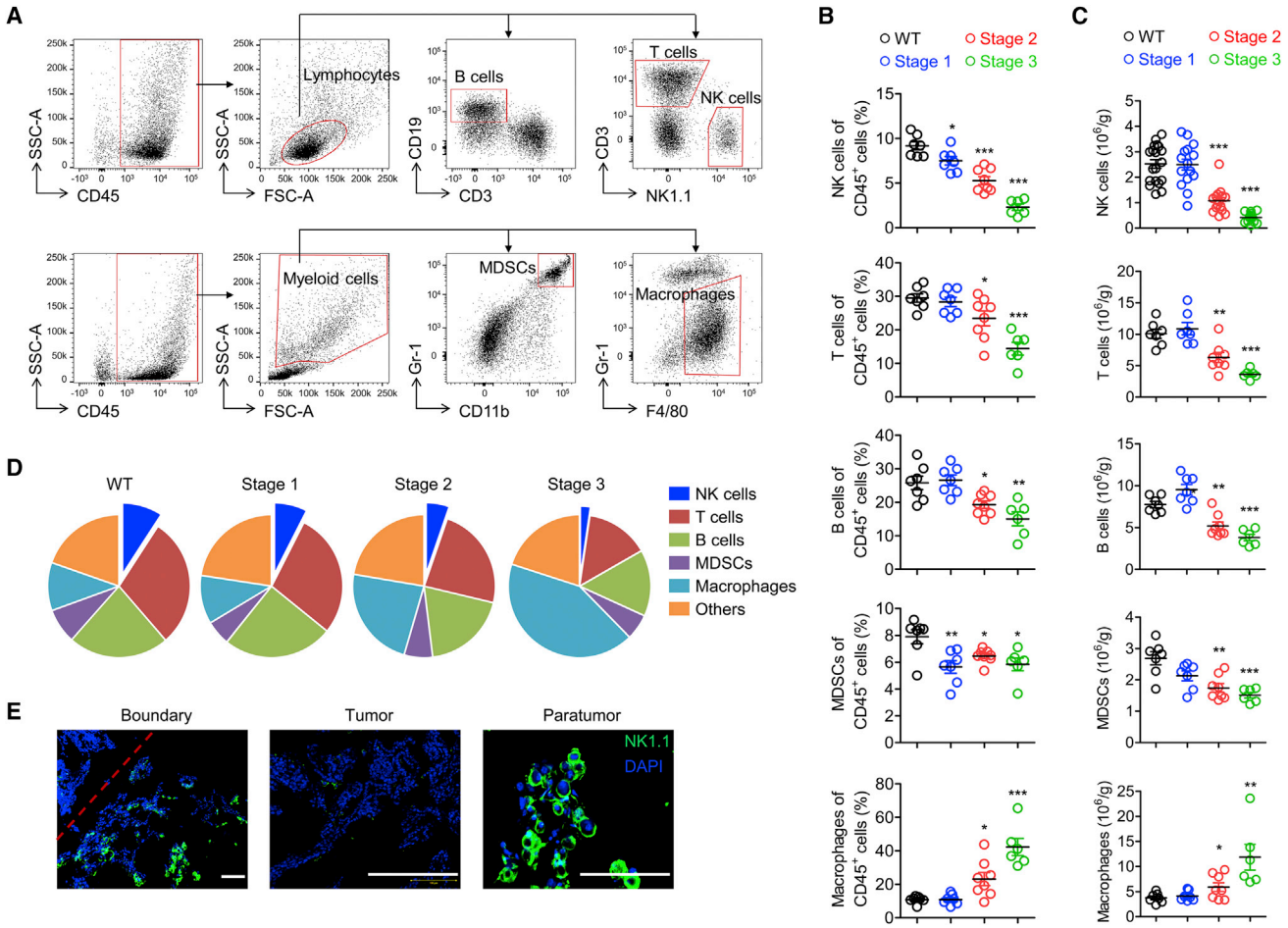

Figure 2. The Number of Lung NK Cells Declines Drastically during Lung Cancer Progression

(A) FCM gating strategy.

(B and C) Quantification of NK cells, T cells, B cells, MDSCs, and macrophages in the lungs; n = 13–19 for the NK cells group in (C); n = 6–8 for other groups. Data are pooled from seven independent experiments.

(D) Pie-chart representation of the composition of leukocytes in the lungs.

(E) Immunofluorescence analyses of NK cells in tumor tissue. Dashed line marks the boundary between tumor and paratumor. Results are representative of three independent experiments. Scale bar, 100 μm.

Each symbol in (B) and (C) represents an individual mouse. Data are presented as mean ± SEM. Unpaired t test, *p < 0.05, **p < 0.01, and ***p < 0.001. See also Figures S1 and S2.

lung cancer microenvironment excludes NK cells profoundly, with a critical time point being during stage 2.

In agreement with previous reports (Xu et al., 2014), a typical macrophage-enriched tumor microenvironment was found in our *Kras* models (Figures 2B–2D). Accumulated macrophages expressed downregulated M1 markers *Il12* and *Tnfα* but upregulated M2 markers *Mrc1* and *Arg1* (Figure S2), indicating their M2-polarized phenotype and their role in promoting lung cancer.

Attenuated Cytotoxicity of NK Cells in the Lung Cancer Microenvironment

To assess the effector functions of NK cells, we examined their cytotoxicity, surface markers, and effector molecules. When co-cultured with LLC or YAC-1 target cells, stage 2 and stage 3 lung NK cells showed significantly attenuated cytotoxicity compared with WT lung NK cells (Figure 3A), whereas the cytotoxicity of spleen NK cells was unchanged during lung cancer development (Figure 3B).

Next, we characterized the markers associated with degranulation, cytokine production, and activation of NK cells. Expression of granzyme B, perforin, CD107a, IFN-γ, and TNF-α was reduced gradually in lung NK cells during lung cancer development (Figures 3C and 3D), suggesting impaired degranulation, and reduced cytokine production in NK cells during lung cancer promotion and progression. Stage 2 and stage 3 lung NK cells expressed lower levels of the cytotoxic receptor CD27, activating receptor NKG2D, and higher levels of the inhibitory receptor NKG2A (Figures 3C and 3D). Furthermore, four subsets of NK cells ($CD27^{-}CD11b^{-}$, $CD27^{+}CD11b^{-}$, $CD27^{+}CD11b^{+}$, and $CD27^{-}CD11b^{+}$) decreased uniformly in number as lung cancer developed. Although IFN-γ and TNF-α were expressed

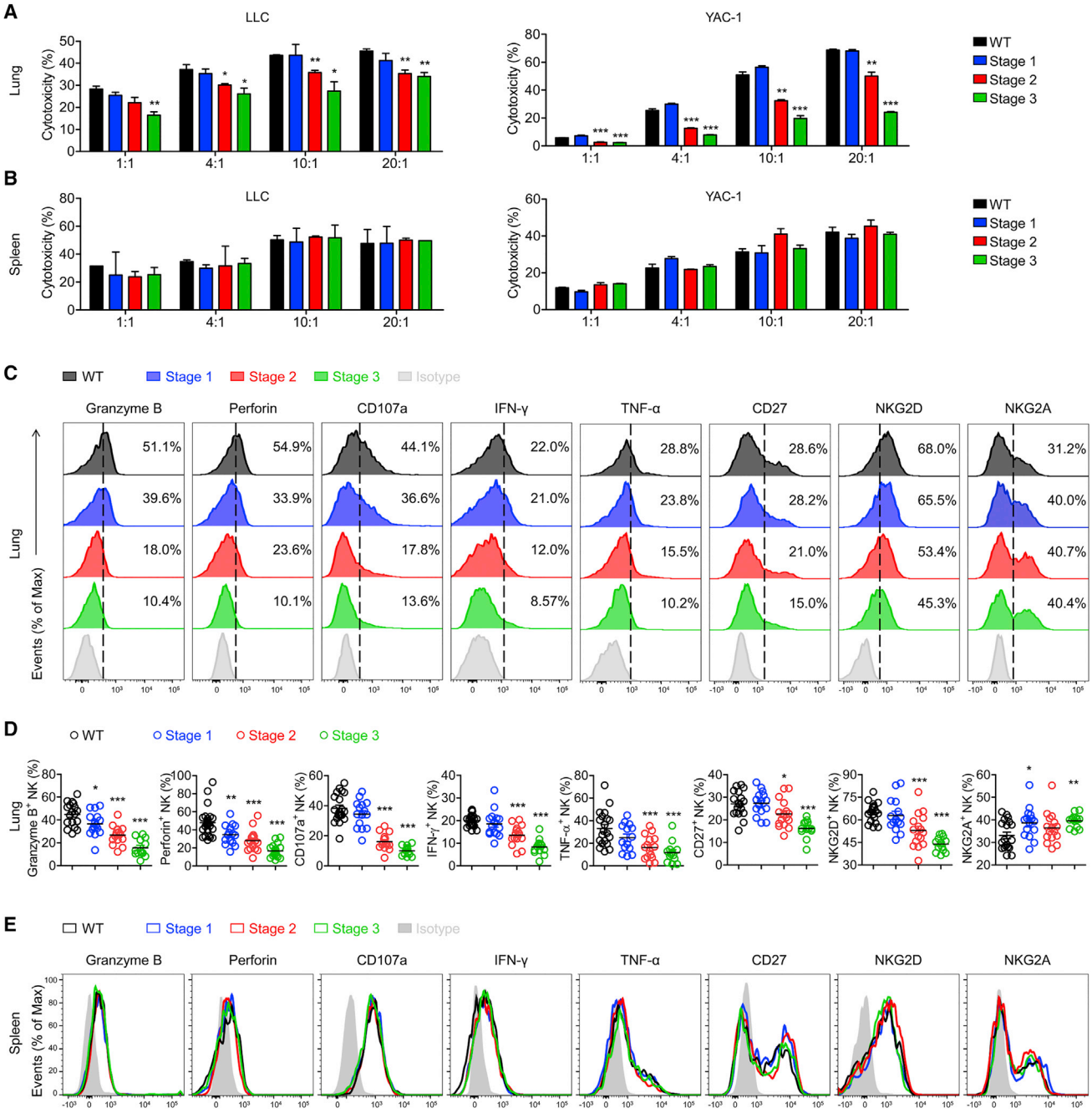

Figure 3. Attenuated Cytotoxicity and Altered Phenotypes of NK Cells in the Lung Cancer Microenvironment

(A and B) Cytotoxicity of purified lung NK (A) and spleen NK (B) cells against LLC and YAC-1 target cells at the indicated ratios (NK cells/target cells); n = 3.

(C and D) Representative histograms (C) and quantification (D) of expression of indicated molecules in lung NK cells. Each symbol represents an individual mouse; n = 13–20. Data are pooled from seven independent experiments.

(E) Representative histograms of indicated molecules in spleen NK cells. Results are representative of three independent experiments.

Data in (A), (B), and (D) are presented as mean ± SEM. Unpaired t test, *p < 0.05, **p < 0.01, and ***p < 0.001. See also Figures S3 and S4.

differently in the four subsets of WT lung NK cells, they were downregulated uniformly in the four subsets of NK cells as lung cancer developed, together with granzyme B, perforin, CD107a, NKG2D, and NKG2D, which were similarly expressed in the four subsets of lung NK cells (Figures S3A and S3B). In agreement with unchanged cytotoxicity, expression of these markers in spleen NK cells did not change (Figure 3E). Therefore, this hyporesponsive state, together with attenuated cytotoxicity, implies the diminished effector functions of NK cells in the lung cancer microenvironment.

In addition to NK cells, diminished effector functions were also observed in T cells, as demonstrated by a lower proportion of $CD8^+$ T cells; a higher proportion of T regulatory cells (Tregs); lower levels of TNF-α, IFN-γ, CD107a, granzyme B, and perforin; and higher levels of CTLA4, PD-1, CD69, and CD44 in the lung cancer microenvironment (Figure S4).

Lung NK cells uniformly expressed CD49b but did not express CD49a, CD127, or TRAIL at different stages of lung cancer, confirming that they were conventional NK cells rather than type 1 innate lymphoid cells. Some studies have found that intratumoral NK cells in humans and mice express increased levels of Tim-3, PD-1, and PD-L1 and decreased levels of CD16, NKp46, and CD226 (Benson et al., 2010; da Silva et al., 2014; Iraolagoitia et al., 2016; Krneta et al., 2016; Pasero et al., 2016; Platonova et al., 2011). However, in our models, the expression of the molecules associated with activation and cytotoxicity, such as NKp46, CD69, CD44, CD226, CD16/32, FasL, TRAIL, CD122, and the inhibitory molecules CTLA4, CD96, CD94, PD-1, PD-L1, Tim3, CD276, LAG3, and CD244 in lung NK cells were unchanged during lung cancer development (Figure S3C), indicating the unique phenotypes of NK cells in *Kras*-driven lung cancer.

Impaired Viability of NK Cells in the Lung Cancer Microenvironment

Given the drastic loss of NK cells during lung cancer promotion and progression, we investigated whether the lung cancer microenvironment influenced the viability of NK cells. As expected, NK cells displayed a gradual decrease in proliferation capacity, as shown by reduced Ki67 expression during lung cancer promotion and progression (Figure 4A). Furthermore, when cultured with IL-2 for 5 days *in vitro*, purified lung NK cells from stage 2 and stage 3 *Kras* mice exhibited significantly impaired viability, and the remaining living cells displayed markedly impaired proliferation capacity. However, purified lung NK cells from stage 1 *Kras* mice exhibited slightly impaired viability and unaffected proliferation capacity (Figure 4B).

Several studies have reported that endogenous and exogenous ROS induces apoptosis of NK cells (Mellqvist et al., 2000; Song et al., 2011). Notably, we found that the intracellular ROS level of NK cells in the lung cancer microenvironment increased significantly, in accordance with their impaired viability. No difference in ROS levels, however, was observed in spleen NK cells (Figure 4C).

To gain further mechanistic insights into these findings, we isolated NK cells from the spleens and lungs of WT and stage 3 *Kras* mice for whole-genome transcriptome analyses by microarrays. Stage 3 lung NK cells displayed the most obvious alterations relative to WT lung NK cells, so comparing these different lung NK cells may provide an insight into the underlying mechanisms. We selected and compared the differentially expressed genes known to be related to the positive regulation of apoptosis and the negative regulation of cell growth to assess the viability and apoptosis of NK cells. A total of 107 differentially expressed genes related to the positive regulation of apoptosis was found in lung NK cells, among which the expression of as many as 85 genes was upregulated substantially in stage 3 lung NK cells, and expression of only 22 genes was upregulated slightly in WT lung NK cells (Figure 4D). These findings suggested that apoptosis of stage 3 NK cells was enhanced significantly. Meanwhile, there was an increase in the expression of differentially expressed genes related to the negative regulation of cell growth in stage 3 lung NK cells compared with that in WT lung NK cells. Of these, there was a 69-fold increase in *Fbp1* expression (Figure 4E), implying its important role in regulating the viability of NK cells. Thus, these results demonstrate the impaired viability of NK cells in the lung cancer microenvironment.

Collectively, the diminished effector functions and impaired viability signifies NK cell dysfunction in the lung cancer microenvironment.

Increased FBP1 Expression Is Concomitant with Decreased Glycolysis in NK Cells

Glucose metabolism is essential for the function of human and mouse NK cells (Assmann et al., 2017; Keating et al., 2016), so dysregulation of glucose metabolism could lead to NK cell dysfunction. To identify the previously unknown metabolic mechanisms involved in NK cell dysfunction, we analyzed the genes associated with glucose metabolism, focusing on *Fbp1*, the expression of which was upregulated robustly in stage 3 lung NK cells (Figure 5A). Using immunofluorescence, FBP1 was detected and localized in the cytoplasm of purified stage 3 lung NK cells but was undetected in WT lung NK cells (Figure 5B). This difference in expression was confirmed using western blotting (Figure 5C). To determine the correlation between *Fbp1* expression and lung cancer development, we purified NK cells from the lungs and spleens of WT and *Kras* mice at different stages of lung cancer to carry out PCR. Notably, expression of FBP1 mRNA was increased gradually during lung cancer development (Figures 5D and 5E), implying that upregulated expression of *Fbp1* in NK cells is associated with an advanced tumor stage. As a control, spleen NK cells did not express *Fbp1* (Figures 5A and 5D). Considering that expression of the immunosuppressive cytokine TGF-β is increased frequently in tumors and is associated with the regulation of NK cell functions (Flavell et al., 2010), we investigated whether upregulation of FBP1 expression was induced by TGF-β. We found that TGF-β expression was increased markedly in the lung cancer microenvironment (Figures S5A and S5B). Lung NK cells were then isolated from WT mice and stimulated with TGF-β, which caused significant upregulation of expression of *Fbp1* mRNA in NK cells (Figure S5C). These data suggest that upregulation of FBP1 expression in NK cells may be caused by tumor microenvironment-derived TGF-β.

FBP1 plays important parts in glucose metabolism and has been shown to inhibit glycolysis in human tumor cells and hematopoietic progenitor cells (Dong et al., 2013; Guo et al., 2018; Hirata et al., 2016; Li et al., 2014). Increased FBP1 expression in NK cells was evident during lung cancer progression, so we investigated whether glycolysis in NK cells was inhibited. The extracellular acidification rate (ECAR) of NK cells isolated from the lungs and spleens of WT and stage 3 *Kras* mice following IL-2 and IL-12 stimulation for 18 hr was measured to evaluate glycolysis. As expected, stage 3 lung NK cells had considerably reduced basal glycolysis relative to those of WT lung NK cells. Addition of glucose and 2-deoxy-D-glucose (2DG; a glycolysis inhibitor) enhanced and reduced the glycolysis of WT lung NK

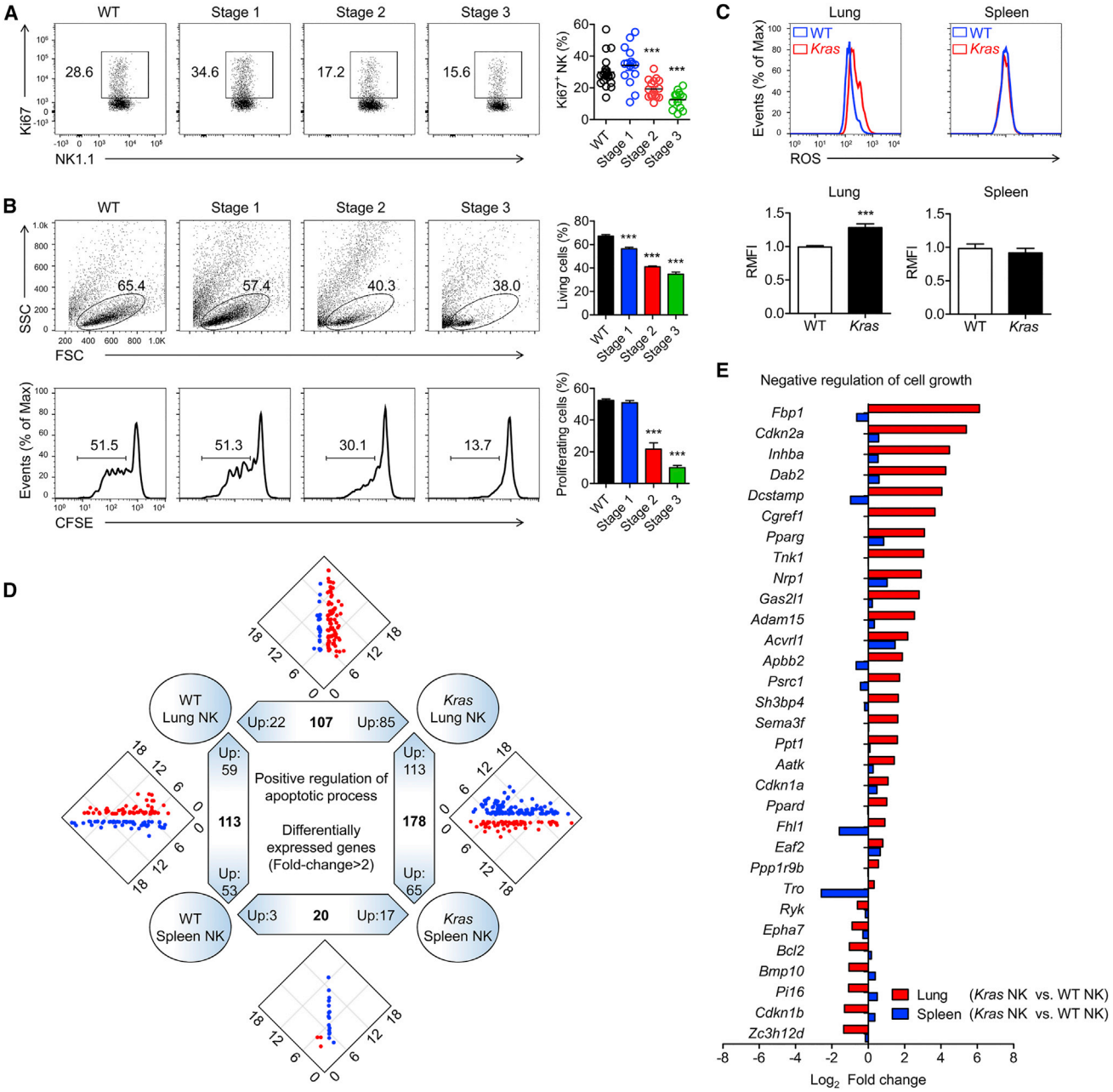

Figure 4. Impaired Viability of NK Cells in the Lung Cancer Microenvironment

(A) Representative FCM plots and quantification of Ki67 expression in lung NK cells. Each symbol represents an individual mouse; n = 20, 15, 16, and 13, respectively. Data are pooled from seven independent experiments.

(B) Purified lung NK cells were cultured with IL-2 for 5 days. Representative FCM profiles and percentages of living NK cells and proliferating NK cells are shown; n = 16, 10, 10, and 16, respectively. Data are pooled from three independent experiments.

(C) Representative histograms and the relative mean fluorescence intensity (RMFI) of intracellular ROS; n = 14 for WT lung and *Kras* lung groups; n = 7 for WT spleen and *Kras* spleen groups. Data are pooled from two independent experiments.

(D and E) Lung and spleen NK cells were isolated from WT mice and stage 3 *Kras* mice for whole-genome transcriptome analyses by microarrays. (D) Scatterplots show differentially expressed genes (fold change >2) related to the positive regulation of apoptotic process. The number of differentially expressed genes is shown in the middle of bidirectional arrows, and the number of highly expressed genes is shown at the end of bidirectional arrows. Axis labels are $\log_2$ normalized; n = 2. (E) Bar graph showing expression of differentially expressed genes related to the negative regulation of cell growth; n = 2.

Data in (A) to (C) are presented as mean ± SEM. Unpaired *t* test, ***p < 0.001.

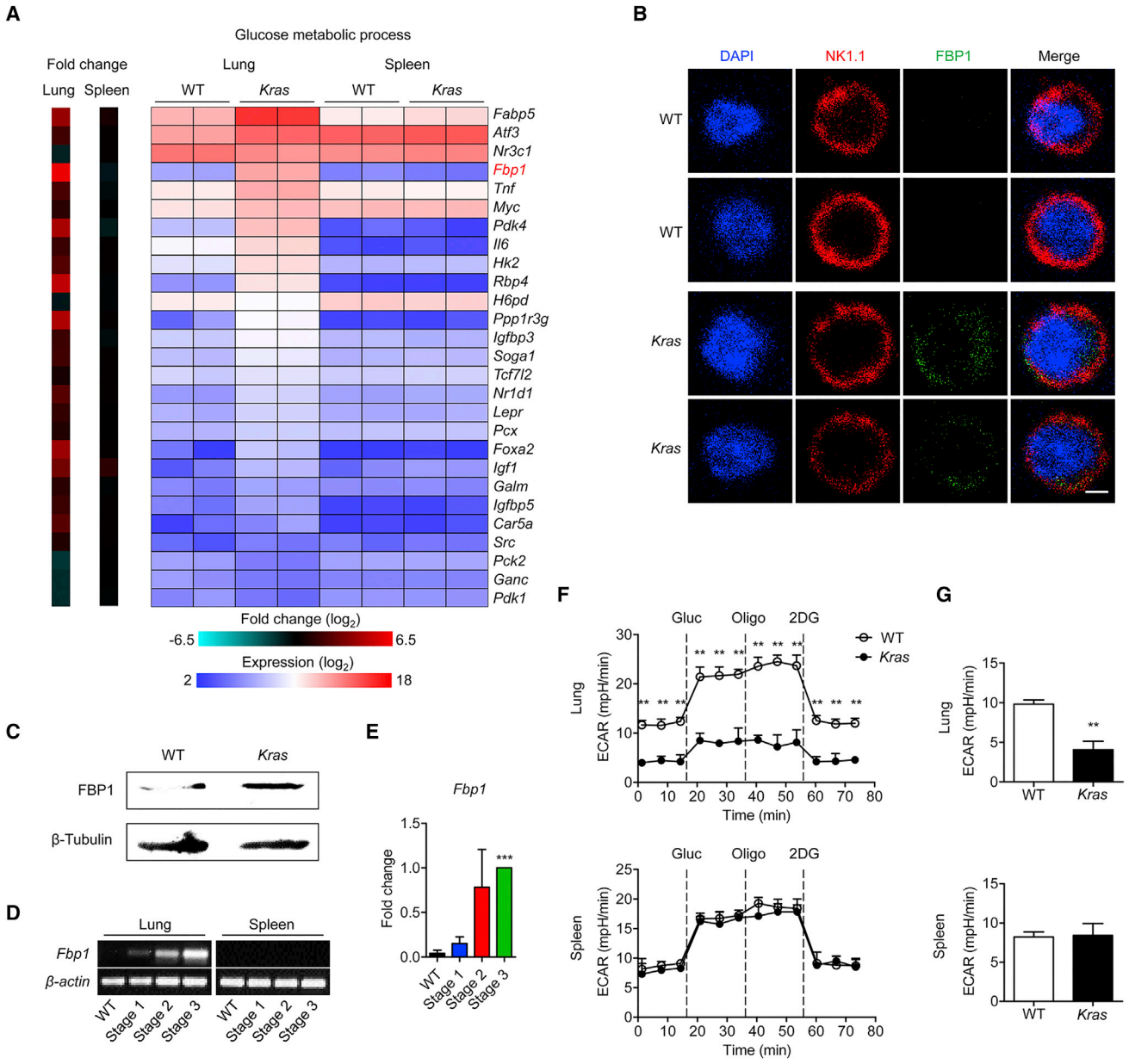

Figure 5. Increased FBP1 Expression and Decreased Glycolysis in NK Cells in the Lung Cancer Microenvironment

(A) Microarrays shown in Figure 4D are detailed. Expression (right) and fold change (left and middle, *Kras* NK cells relative to WT NK cells) of the genes associated with glucose metabolic process are shown.

(B and C) Immunofluorescence (B) and western blotting (C) of FBP1 expression in lung NK cells isolated from WT and stage 3 *Kras* mice. Scale bar, 2 μm.

(D) Analyses of *Fbp1* mRNA expression in purified lung NK cells by RT-PCR. One of two independent experiments is shown.

(E) Analyses of *Fbp1* mRNA expression in purified lung NK cells by qRT-PCR; n = 5. Data are pooled from five independent experiments.

(F and G) ECAR of lung and spleen NK cells isolated from WT and stage 3 *Kras* mice was assessed by the Seahorse assay in triplicate or quadruplicate. (F) Representative plots of ECAR over time with the addition of glucose, oligomycin A, and 2DG, as indicated. (G) Basal glycolysis was determined after addition of glucose. n = 3–4. Results are representative of three independent experiments.

Data in (E) to (G) are presented as mean ± SEM. Unpaired t test, $^{**}p < 0.01$ and $^{***}p < 0.001$. See also Figure S5.

cells significantly, respectively, but had little effect on stage 3 lung NK cells. In addition, the real-time ECAR values of stage 3 lung NK cells were consistently lower than those of WT lung NK cells (Figures 5F and 5G). As a control, the glycolysis of spleen NK cells was measured and remained unchanged (Figures 5F and 5G). Collectively, these results suggest that NK cells show increased FBP1 expression and concomitant decreased glycolysis in the lung cancer microenvironment.

Inhibition of FBP1 Restores the Function of NK Cells

Glycolysis has been reported to be important for immune cell function, especially in activated cells and effector cells, including

activated NK cells (Donnelly et al., 2014; O'Neill et al., 2016). Given the observation that NK cells show higher levels of FBP1 expression and lower levels of glycolysis in the lung cancer environment, we hypothesized that dysfunction of NK cells could be mediated by FBP1 through glycolysis inhibition. First, we examined whether inhibition of FBP1 could enhance the glycolysis of dysfunctional NK cells. Considering that stage 3 lung NK cells were in an exceedingly dysfunctional state with minimal glycolysis and that this extremely arduous state could be irreversible, we used stage 2 lung NK cells, which were in a mildly dysfunctional state. NK cells were isolated from the lungs and spleens of WT and stage 2 *Kras* mice and stimulated with IL-2 and IL-12 for 18 hr in the presence of MB05032 (FBP1 inhibitor) or DMSO (control) (Erion et al., 2005). As expected, stage 2 lung NK cells treated with MB05032 displayed significantly enhanced glycolysis compared with the DMSO group (Figures 6A and 6B). As a control, spleen NK cells, which do not express FBP1, displayed no difference (Figures S6A and S6B), showing that FBP1 inhibited glycolysis in NK cells directly.

Next, we investigated the effect of FBP1 on the effector functions and viability of NK cells. As expected, FBP1 inhibition increased the cytotoxicity (Figure 6C) and cytokine-induced activation of stage 2 lung NK cells (Figure 6D). In addition, the viability and proliferation capacity of stage 2 lung NK cells were improved to some extent (Figure 6E), and ROS generation was reduced after treatment with MB05032 (Figure 6F). As a control, FBP1 inhibition did not influence the cytotoxicity or viability of spleen NK cells (Figures S6C and S6D). These results show that FBP1 inhibits the effector functions and viability of NK cells, at least in part. Frustratingly, but not surprisingly, the effector functions and viability of stage 3 lung NK cells were not restored by inhibiting FBP1 (Figures S6E and S6F). Furthermore, we undertook adoptive transfer of NK cells and found that transfer of NK cells treated with MB05032 immediately slowed tumor growth compared with the DMSO group (Figure 6G). These data demonstrate that FBP1 plays an important part in promoting tumor development by inhibiting NK cell functions.

To ascertain whether the effect of FBP1 on NK cells was dependent upon glycolysis, we assessed the cytotoxicity and viability of NK cells treated simultaneously with MBO5032 and 2DG. We found that inhibition of FBP1 failed to restore the cytotoxicity of stage 2 lung NK cells after addition of 2DG (Figure 6H), whereas inhibition of FBP1 consistently improved the viability of such cells with or without 2DG (Figure 6I). Thus, FBP1 weakens the cytotoxicity of NK cells by inhibition of glycolysis, but FBP1 impairs the viability of NK cells directly independent of glycolysis.

DISCUSSION

In summary, we provided a comprehensive analysis of NK cells through all stages of tumor development in *Kras*-driven lung cancer. We demonstrated that NK cells prevent tumor initiation but gradually lose their antitumor effect as the tumor develops. FBP1-induced NK cell dysfunction during lung cancer promotion and progression was involved intricately in this finding. Importantly, FBP1 inhibition could, at least in part, restore NK cell function. We revealed that FBP1 is a key regulator in NK cell dysfunction. These findings could help to guide clinical treatment. The research presented in this report provides three main insights into the function and dysfunction of NK cells during tumor development.

First, we demonstrated that the functional status of NK cells is closely related to the course of tumor development, as well as their antitumor effect, and we clearly presented the overall process of NK cells from a functional state to a dysfunctional state using a *Kras* mouse model. In liver cancer in mice, tumor-specific T cell dysfunction is a dynamic differentiation program. Initially, the dysfunctional state of tumor-specific T cells is therapeutically reversible but, ultimately, becomes a fixed state (Philip et al., 2017; Schietinger et al., 2016). Similarly, we showed that NK cells in the mouse lung cancer microenvironment behaved in an analogous manner. During tumor initiation (stage 1), NK cells were fully functional with robust cytotoxicity and viability and could eliminate tumor cells potently. During tumor promotion (stage 2), NK cells were in a mild dysfunctional state that could be reversed by FBP1 inhibition. At this stage, NK cells were in equilibrium with tumor cells. During tumor progression (stage 3), NK cells evolved into an extreme and incurable dysfunctional state with significantly impaired cytotoxicity and viability that could not be reversed by FBP1 inhibition. Tumor cells opposed NK cells and escaped from NK cell-mediated immunosurveillance. Moreover, only lung NK cells, but not systemic NK cells, showed dynamic alterations, revealing that the tumor microenvironment affected NK cells profoundly. Taken together, the interrelationships between NK cells and tumor cells over the course of tumor development also confirmed the cancer immunoediting theory (Dunn et al., 2002).

Considerable research about the powerful antitumor effect of human and mouse NK cells has been reported (Malmberg et al., 2017; Vivier et al., 2008), but some investigators have found that the presence of NK cells does not correlate with clinical outcome in esophageal carcinoma or NSCLC (Platonova et al., 2011; Senovilla et al., 2012); therefore, the role of NK cells in controlling tumors remains controversial. We were able to resolve this controversy, at least in *Kras*-driven lung cancer in mice. We demonstrated that NK cells exhibited an inconsistent antitumor effect depending on the stage of lung cancer. NK cells prevented tumor initiation effectively but failed to control tumor promotion and progression in *Kras*-driven lung cancer. Accordingly, we speculate that the limited prognostic value of NK cells in esophageal carcinoma and NSCLC is because such patients mainly have tumors at middle or advanced stages, and the effector functions of their intratumoral NK cells have, thus, been impaired severely. This hypothesis is backed up by our observation in *Kras* mice that depletion of NK cells during tumor promotion and progression did not influence the course of tumor development. Collectively, these data present an overall perspective of NK cells during tumor development and provide deep insights into the role of NK cells in controlling tumors.

Second, we provided evidence that the tumor microenvironment "disables" NK cells by weakening their glycolytic metabolism, thus promoting tumor development; remarkably, FBP1 is a key molecule in this process. Hence, we have reported, for the first time, the metabolic reprogramming of NK cells in tumors,

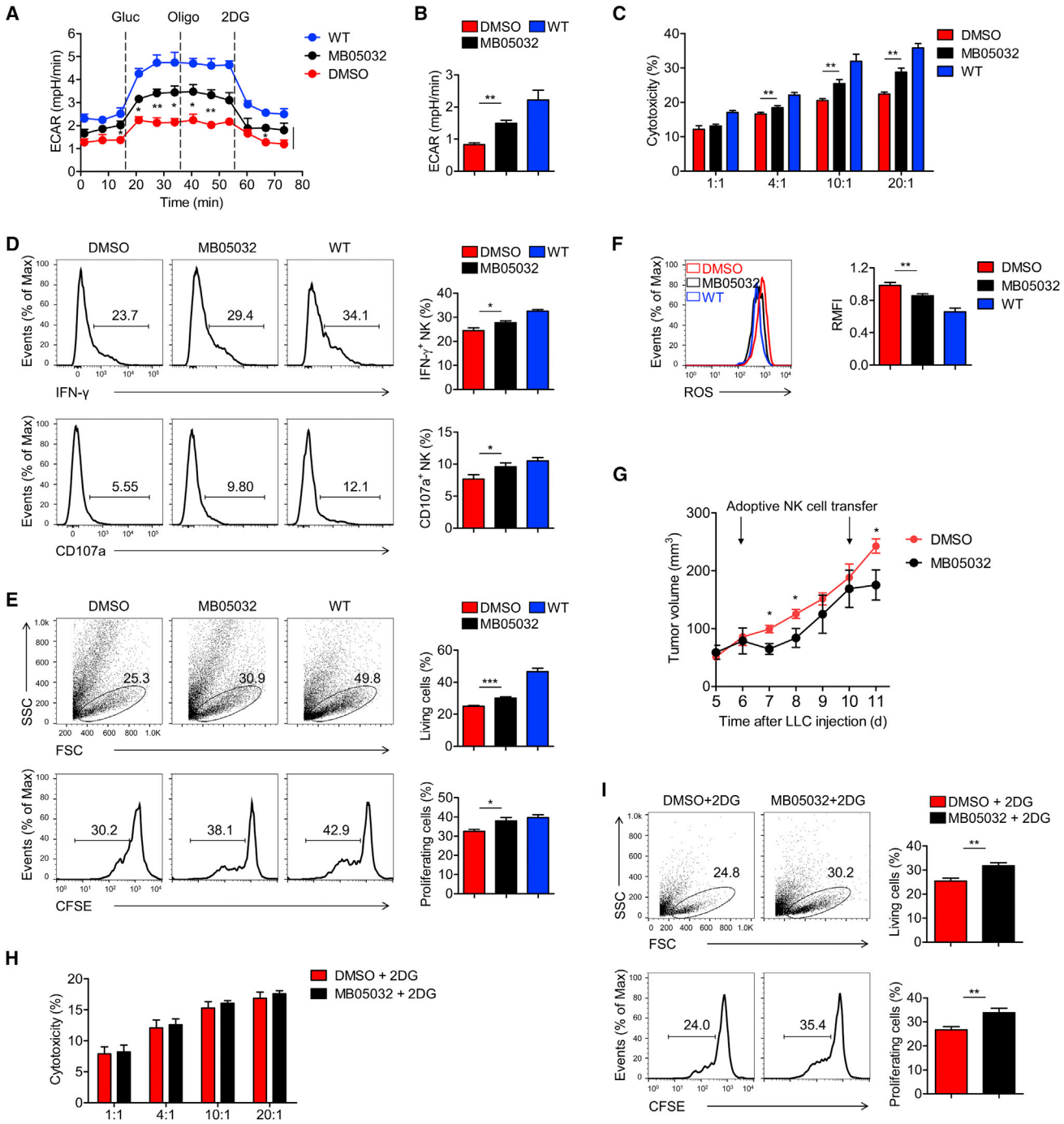

Figure 6. FBP1 Induces NK Cell Dysfunction by Inhibiting Glycolysis and Viability

(A and B) Purified WT and stage 2 lung NK cells were stimulated with IL-2 and IL-12 for 18 hr, with or without MB05032, and ECAR was assessed in triplicate or quadruplicate. (A) Representative plots of EACR over time with the addition of glucose, oligomycin A, and 2DG, as indicated. (B) Basal glycolysis was determined after addition of glucose. n = 3–4. One of two independent experiments is shown.

(C) Purified WT and stage 2 lung NK cells were treated with or without MB05032 for 18 hr. Cytotoxicity against LLC target cells at the indicated ratios (NK cells/target cells) is shown; n = 5. Data are pooled from two independent experiments.

(D) Purified WT and stage 2 lung NK cells were stimulated with IL-2 and IL-12 for 18 hr, with or without MB05032. Representative histograms and quantification of expression of IFN-γ and CD107a are shown; n = 9–11. Data are pooled from two independent experiments.

(E) Purified WT and stage 2 lung NK cells were cultured with IL-2, with or without MB05032, for 5 days. Representative FCM profiles and percentages of living NK cells and proliferating NK cells are shown; n = 11–12. Data are pooled from two independent experiments.

(F) Purified WT and stage 2 lung NK cells were treated with or without MB05032 for 18 hr. Representative histograms and RMFI of intracellular ROS are shown; n = 14. Data are pooled from two independent experiments.

(legend continued on next page)

and this result may provide a useful complement to the current immune escape theory. Metabolic changes can control the course of immune responses directly (Biswas, 2015; Gardiner and Finlay, 2017; O'Neill et al., 2016). In mice, NK cells have been shown to increase glycolysis upon activation (Assmann et al., 2017; Donnelly et al., 2014; Keppel et al., 2015; Kobayashi and Mattarollo, 2017; Marcais et al., 2014). On the other hand, we found that NK cells in a hyporesponsive and dysfunctional state displayed diminished glycolysis, which influenced the effector functions of NK cells in the mouse tumor microenvironment. Moreover, the tumor microenvironment upregulated FBP1 expression in NK cells. This led to NK cell dysfunction by inhibiting glycolysis and impairing the viability of NK cells, which accounted for the gaps in relevance between FBP1 and the immune system. FBP1 is a pivotal gluconeogenic enzyme, so the effect of gluconeogenesis on NK cells deserves further investigation. Taken together, these observations broaden our understanding of the metabolic pathways in NK cells in different conditions and probably reflect a previously unknown mechanism of immune escape.

Third, we showed that FBP1 inhibition during tumor promotion, but not tumor progression, can restore NK cell function, at least in part. NK cell-based cancer immunotherapy, especially adoptive NK cell therapy, is garnering considerable interest because NK cells can facilitate the adaptive immune response by secreting cytokines and kill tumor cells directly without prior encounter or sensitization with antigens (Chu et al., 2014; Fan et al., 2006; Guillerey et al., 2016). However, some research teams have reported that adoptive transfer of NK cells does not mediate tumor regression in patients with metastatic melanoma or renal cell carcinoma because NK cells are in a dysfunctional state and lose their capacity to lyse tumor cells *in vivo* (Parkhurst et al., 2011). Therefore, deeper understanding of the mechanisms involved in the function and dysfunction of NK cells in the unique tumor microenvironment and enhancement of the effector functions of NK cells *in vivo*, will improve the efficacy of NK cell-based cancer immunotherapy. Our results highlight a novel strategy and indicate the key timing to enhance the effector functions of tumor-infiltrating NK cells, thus providing novel information for NK cell-based cancer immunotherapy.

Limitations of the Study

Despite such insights, we are well aware of some limitations of our study. Our results showed that NK cells are gradually induced into a dysfunctional state and increasingly lose their antitumor effect during tumor development in a *Kras*-driven model of spontaneous lung cancer. These phenomena were closely associated with FBP1-induced inhibition of glycolysis and impaired viability. However, whether these phenomena and mechanisms can be extended to other mouse lung cancer types and human *KRAS* mutant lung cancer is unsolved. Moreover, more effective immunotherapies involving FBP1 targeting deserve further study.

STAR★METHODS

Detailed methods are provided in the online version of this paper and include the following:

- KEY RESOURCES TABLE
- CONTACT FOR REAGENT AND RESOURCE SHARING
- EXPERIMENTAL MODEL AND SUBJECT DETAILS
  - Mice
  - Cell Lines
  - Plasmids
- METHOD DETAILS
  - *In Vivo* Experiments
  - Isolation of Leukocytes, NK Cells, and Macrophages
  - Flow Cytometry and Antibodies
  - Cytokine-Induced Activation of NK Cells
  - TGF-β Stimulation
  - ELISA
  - Viability and Proliferation Assay
  - Cytotoxicity Assay
  - ECAR Analyses
  - ROS Analyses
  - Analyses of Gene Expression
  - Histology
  - Immunofluorescence
  - Western Blotting
- QUANTIFICATION AND STATISTICAL ANALYSIS
- DATA AND SOFTWARE AVAILABILITY

SUPPLEMENTAL INFORMATION

Supplemental Information includes six figures and can be found with this article online at https://doi.org/10.1016/j.cmet.2018.06.021.

ACKNOWLEDGMENTS

This work was supported by the key project of the National Natural Science Foundation of China (81330071, 81788101, 91442202, and 81602491) and The Strategic Priority Research Program of the Chinese Academy of Sciences (CAS grants XDA12020217, XDPB10).

AUTHOR CONTRIBUTIONS

J.C. designed and conducted experiments, analyzed data, and wrote the manuscript. X.W. and D.W. conducted some experiments. X.W., X.Z., and B.F. provided advice. R.S. established techniques of flow cytometry and interpreted the data. Z.T. and H.W. designed the study, supervised the research, and revised the manuscript.

(G) A total of 8×10^5 LLC cells were injected (subcutaneously) into WT mice. Purified stage 2 lung NK cells were treated with MB05032 or DMSO for 18 hr, and injected into subcutaneous tumors (3×10^5/25 μL/mouse) 6 and 10 days after subcutaneous injection of LLC cells. Tumor growth curves are shown; n = 5.
(H) Purified stage 2 lung NK cells were treated with 2DG, with or without MB05032, for 18 hr. Cytotoxicity against LLC target cells at the indicated ratios (NK cells/target cells) is shown; n = 5. Data are pooled from two independent experiments.
(I) Purified WT and stage 2 lung NK cells were cultured with IL-2 and 2DG, with or without MB05032, for 5 days. Representative FCM profiles and percentages of living NK cells and proliferating NK cells are shown; n = 8. Data are pooled from two independent experiments.
Data in (A) to (I) are presented as mean ± SEM. Unpaired t test, *p < 0.1, **p < 0.01, and ***p < 0.001. See also Figures S6.

DECLARATION OF INTERESTS

The authors declare no competing interests.

Received: October 10, 2017
Revised: April 8, 2018
Accepted: June 25, 2018
Published: July 19, 2018

REFERENCES

Assmann, N., O'Brien, K.L., Donnelly, R.P., Dyck, L., Zaiatz-Bittencourt, V., Loftus, R.M., Heinrich, P., Oefner, P.J., Lynch, L., Gardiner, C.M., et al. (2017). Srebp-controlled glucose metabolism is essential for NK cell functional responses. Nat. Immunol. *18*, 1197–1206.

Benson, D.M., Jr., Bakan, C.E., Mishra, A., Hofmeister, C.C., Efebera, Y., Becknell, B., Baiocchi, R.A., Zhang, J., Yu, J., Smith, M.K., et al. (2010). The PD-1/PD-L1 axis modulates the natural killer cell versus multiple myeloma effect: a therapeutic target for CT-011, a novel monoclonal anti-PD-1 antibody. Blood *116*, 2286–2294.

Biswas, S.K. (2015). Metabolic reprogramming of immune cells in cancer progression. Immunity *43*, 435–449.

Bjorkstrom, N.K., Ljunggren, H.G., and Michaelsson, J. (2016). Emerging insights into natural killer cells in human peripheral tissues. Nat. Rev. Immunol. *16*, 310–320.

Brahmer, J.R., Tykodi, S.S., Chow, L.Q., Hwu, W.J., Topalian, S.L., Hwu, P., Drake, C.G., Camacho, L.H., Kauh, J., Odunsi, K., et al. (2012). Safety and activity of anti-PD-L1 antibody in patients with advanced cancer. N. Engl. J. Med. *366*, 2455–2465.

Bruno, A., Focaccetti, C., Pagani, A., Imperatori, A.S., Spagnoletti, M., Rotolo, N., Cantelmo, A.R., Franzi, F., Capella, C., Ferlazzo, G., et al. (2013). The proangiogenic phenotype of natural killer cells in patients with non-small cell lung cancer. Neoplasia *15*, 133–142.

Carrega, P., Morandi, B., Costa, R., Frumento, G., Forte, G., Altavilla, G., Ratto, G.B., Mingari, M.C., Moretta, L., and Ferlazzo, G. (2008). Natural killer cells infiltrating human nonsmall-cell lung cancer are enriched in $CD56^{bright}$ $CD16^{-}$ cells and display an impaired capability to kill tumor cells. Cancer *112*, 863–875.

Chen, M., Zhang, J., Li, N., Qian, Z., Zhu, M., Li, Q., Zheng, J., Wang, X., and Shi, G. (2011). Promoter hypermethylation mediated downregulation of FBP1 in human hepatocellular carcinoma and colon cancer. PLoS One *6*, e25564.

Chen, Z., Fillmore, C.M., Hammerman, P.S., Kim, C.F., and Wong, K.K. (2014). Non-small-cell lung cancers: a heterogeneous set of diseases. Nat. Rev. Cancer *14*, 535–546.

Chu, J., Deng, Y., Benson, D.M., He, S., Hughes, T., Zhang, J., Peng, Y., Mao, H., Yi, L., Ghoshal, K., et al. (2014). CS1-specific chimeric antigen receptor (CAR)-engineered natural killer cells enhance in vitro and in vivo antitumor activity against human multiple myeloma. Leukemia *28*, 917–927.

Culley, F.J. (2009). Natural killer cells in infection and inflammation of the lung. Immunology *128*, 151–163.

da Silva, I.P., Gallois, A., Jimenez-Baranda, S., Khan, S., Anderson, A.C., Kuchroo, V.K., Osman, I., and Bhardwaj, N. (2014). Reversal of NK-cell exhaustion in advanced melanoma by Tim-3 blockade. Cancer Immunol. Res. *2*, 410–422.

Dong, C., Yuan, T., Wu, Y., Wang, Y., Fan, T.W., Miriyala, S., Lin, Y., Yao, J., Shi, J., Kang, T., et al. (2013). Loss of FBP1 by Snail-mediated repression provides metabolic advantages in basal-like breast cancer. Cancer Cell *23*, 316–331.

Donnelly, R.P., Loftus, R.M., Keating, S.E., Liou, K.T., Biron, C.A., Gardiner, C.M., and Finlay, D.K. (2014). mTORC1-dependent metabolic reprogramming is a prerequisite for NK cell effector function. J. Immunol. *193*, 4477–4484.

Dunn, G.P., Bruce, A.T., Ikeda, H., Old, L.J., and Schreiber, R.D. (2002). Cancer immunoediting: from immunosurveillance to tumor escape. Nat. Immunol. *3*, 991–998.

DuPage, M., Dooley, A.L., and Jacks, T. (2009). Conditional mouse lung cancer models using adenoviral or lentiviral delivery of Cre recombinase. Nat. Protoc. *4*, 1064–1072.

Emery, J.L., Howat, A.J., Variend, S., and Vawter, G.F. (1988). Investigation of inborn errors of metabolism in unexpected infant deaths. Lancet *2*, 29–31.

Erion, M.D., van Poelje, P.D., Dang, Q., Kasibhatla, S.R., Potter, S.C., Reddy, M.R., Reddy, K.R., Jiang, T., and Lipscomb, W.N. (2005). MB06322 (CS-917): a potent and selective inhibitor of fructose 1,6-bisphosphatase for controlling gluconeogenesis in type 2 diabetes. Proc. Natl. Acad. Sci. USA *102*, 7970–7975.

Fan, Z., Yu, P., Wang, Y., Wang, Y., Fu, M.L., Liu, W., Sun, Y., and Fu, Y.X. (2006). NK-cell activation by LIGHT triggers tumor-specific CD8+ T-cell immunity to reject established tumors. Blood *107*, 1342–1351.

Flavell, R.A., Sanjabi, S., Wrzesinski, S.H., and Licona-Limon, P. (2010). The polarization of immune cells in the tumour environment by TGFbeta. Nat. Rev. Immunol. *10*, 554–567.

Fridman, W.H., Pages, F., Sautes-Fridman, C., and Galon, J. (2012). The immune contexture in human tumours: impact on clinical outcome. Nat. Rev. Cancer *12*, 298–306.

Gardiner, C.M., and Finlay, D.K. (2017). What fuels natural killers? metabolism and NK cell responses. Front Immunol. *8*, 367.

Gregoire, C., Chasson, L., Luci, C., Tomasello, E., Geissmann, F., Vivier, E., and Walzer, T. (2007). The trafficking of natural killer cells. Immunol. Rev. *220*, 169–182.

Guillerey, C., Huntington, N.D., and Smyth, M.J. (2016). Targeting natural killer cells in cancer immunotherapy. Nat. Immunol. *17*, 1025–1036.

Guo, B., Huang, X., Lee, M.R., Lee, S.A., and Broxmeyer, H.E. (2018). Antagonism of PPAR-gamma signaling expands human hematopoietic stem and progenitor cells by enhancing glycolysis. Nat. Med. *24*, 360–367.

Hirata, H., Sugimachi, K., Komatsu, H., Ueda, M., Masuda, T., Uchi, R., Sakimura, S., Nambara, S., Saito, T., Shinden, Y., et al. (2016). Decreased expression of fructose-1,6-bisphosphatase associates with glucose metabolism and tumor progression in hepatocellular carcinoma. Cancer Res. *76*, 3265–3276.

Iraolagoitia, X.L., Spallanzani, R.G., Torres, N.I., Araya, R.E., Ziblat, A., Domaica, C.I., Sierra, J.M., Nunez, S.Y., Secchiari, F., Gajewski, T.F., et al. (2016). NK cells restrain spontaneous antitumor CD8+ T cell priming through PD-1/PD-L1 interactions with dendritic cells. J. Immunol. *197*, 953–961.

Keating, S.E., Zaiatz-Bittencourt, V., Loftus, R.M., Keane, C., Brennan, K., Finlay, D.K., and Gardiner, C.M. (2016). Metabolic reprogramming supports IFN-gamma production by CD56bright NK cells. J. Immunol. *196*, 2552–2560.

Keppel, M.P., Saucier, N., Mah, A.Y., Vogel, T.P., and Cooper, M.A. (2015). Activation-specific metabolic requirements for NK Cell IFN-gamma production. J. Immunol. *194*, 1954–1962.

Kishton, R.J., Sukumar, M., and Restifo, N.P. (2017). Metabolic regulation of T cell longevity and function in tumor immunotherapy. Cell Metab. *26*, 94–109.

Kobayashi, T., and Mattarollo, S.R. (2017). Natural killer cell metabolism. Mol. Immunol. https://doi.org/10.1016/j.molimm.2017.11.021.

Krneta, T., Gillgrass, A., Chew, M., and Ashkar, A.A. (2016). The breast tumor microenvironment alters the phenotype and function of natural killer cells. Cell. Mol. Immunol. *13*, 628–639.

Lavin, Y., Kobayashi, S., Leader, A., Amir, E.D., Elefant, N., Bigenwald, C., Remark, R., Sweeney, R., Becker, C.D., Levine, J.H., et al. (2017). Innate immune landscape in early lung adenocarcinoma by paired single-cell analyses. Cell *169*, 750–765.e17.

Li, B., Qiu, B., Lee, D.S., Walton, Z.E., Ochocki, J.D., Mathew, L.K., Mancuso, A., Gade, T.P., Keith, B., Nissim, I., et al. (2014). Fructose-1,6-bisphosphatase opposes renal carcinoma progression. Nature *513*, 251–255.

Malmberg, K.J., Carlsten, M., Bjorklund, A., Sohlberg, E., Bryceson, Y.T., and Ljunggren, H.G. (2017). Natural killer cell-mediated immunosurveillance of human cancer. Semin. Immunol. *31*, 20–29.

Mamessier, E., Sylvain, A., Bertucci, F., Castellano, R., Finetti, P., Houvenaeghel, G., Charaffe-Jaufret, E., Birnbaum, D., Moretta, A., and Olive, D. (2011). Human breast tumor cells induce self-tolerance mechanisms

to avoid NKG2D-mediated and DNAM-mediated NK cell recognition. Cancer Res. *71*, 6621–6632.

Marcais, A., Cherfils-Vicini, J., Viant, C., Degouve, S., Viel, S., Fenis, A., Rabilloud, J., Mayol, K., Tavares, A., Bienvenu, J., et al. (2014). The metabolic checkpoint kinase mTOR is essential for IL-15 signaling during the development and activation of NK cells. Nat. Immunol. *15*, 749–757.

Mellqvist, U.H., Hansson, M., Brune, M., Dahlgren, C., Hermodsson, S., and Hellstrand, K. (2000). Natural killer cell dysfunction and apoptosis induced by chronic myelogenous leukemia cells: role of reactive oxygen species and regulation by histamine. Blood *96*, 1961–1968.

Morvan, M.G., and Lanier, L.L. (2016). NK cells and cancer: you can teach innate cells new tricks. Nat. Rev. Cancer *16*, 7–19.

O'Neill, L.A., Kishton, R.J., and Rathmell, J. (2016). A guide to immunometabolism for immunologists. Nat. Rev. Immunol. *16*, 553–565.

Parkhurst, M.R., Riley, J.P., Dudley, M.E., and Rosenberg, S.A. (2011). Adoptive transfer of autologous natural killer cells leads to high levels of circulating natural killer cells but does not mediate tumor regression. Clin. Cancer Res. *17*, 6287–6297.

Pasero, C., Gravis, G., Guerin, M., Granjeaud, S., Thomassin-Piana, J., Rocchi, P., Paciencia-Gros, M., Poizat, F., Bentobji, M., Azario-Cheillan, F., et al. (2016). Inherent and tumor-driven immune tolerance in the prostate microenvironment impairs natural killer cell antitumor activity. Cancer Res. *76*, 2153–2165.

Philip, M., Fairchild, L., Sun, L., Horste, E.L., Camara, S., Shakiba, M., Scott, A.C., Viale, A., Lauer, P., Merghoub, T., et al. (2017). Chromatin states define tumour-specific T cell dysfunction and reprogramming. Nature *545*, 452–456.

Platonova, S., Cherfils-Vicini, J., Damotte, D., Crozet, L., Vieillard, V., Validire, P., Andre, P., Dieu-Nosjean, M.C., Alifano, M., Regnard, J.F., et al. (2011). Profound coordinated alterations of intratumoral NK cell phenotype and function in lung carcinoma. Cancer Res. *71*, 5412–5422.

Reck, M., Heigener, D.F., Mok, T., Soria, J.C., and Rabe, K.F. (2013). Management of non-small-cell lung cancer: recent developments. Lancet *382*, 709–719.

Roberts, P.J., and Stinchcombe, T.E. (2013). KRAS mutation: should we test for it, and does it matter? J. Clin. Oncol. *31*, 1112–1121.

Robinson, B.W., Pinkston, P., and Crystal, R.G. (1984). Natural killer cells are present in the normal human lung but are functionally impotent. J. Clin. Invest. *74*, 942–950.

Rusakiewicz, S., Semeraro, M., Sarabi, M., Desbois, M., Locher, C., Mendez, R., Vimond, N., Concha, A., Garrido, F., Isambert, N., et al. (2013). Immune infiltrates are prognostic factors in localized gastrointestinal stromal tumors. Cancer Res. *73*, 3499–3510.

Schietinger, A., Philip, M., Krisnawan, V.E., Chiu, E.Y., Delrow, J.J., Basom, R.S., Lauer, P., Brockstedt, D.G., Knoblaugh, S.E., Hammerling, G.J., et al. (2016). Tumor-specific T cell dysfunction is a dynamic antigen-driven differentiation program initiated early during tumorigenesis. Immunity *45*, 389–401.

Senovilla, L., Vacchelli, E., Galon, J., Adjemian, S., Eggermont, A., Fridman, W.H., Sautes-Fridman, C., Ma, Y., Tartour, E., Zitvogel, L., et al. (2012). Trial watch: prognostic and predictive value of the immune infiltrate in cancer. Oncoimmunology *1*, 1323–1343.

Siegel, R., Naishadham, D., and Jemal, A. (2012). Cancer statistics, 2012. CA Cancer J. Clin. *62*, 10–29.

Smyth, M.J., Hayakawa, Y., Takeda, K., and Takeda, K. (2002). New aspects of natural-killer-cell surveillance and therapy of cancer. Nat. Rev. Cancer *2*, 850–861.

Song, H., Park, H., Kim, Y.S., Kim, K.D., Lee, H.K., Cho, D.H., Yang, J.W., and Hur, D.Y. (2011). L-kynurenine-induced apoptosis in human NK cells is mediated by reactive oxygen species. Int. Immunopharmacol. *11*, 932–938.

Topalian, S.L., Hodi, F.S., Brahmer, J.R., Gettinger, S.N., Smith, D.C., McDermott, D.F., Powderly, J.D., Carvajal, R.D., Sosman, J.A., Atkins, M.B., et al. (2012). Safety, activity, and immune correlates of anti-PD-1 antibody in cancer. N. Engl. J. Med. *366*, 2443–2454.

Vivier, E., Tomasello, E., Baratin, M., Walzer, T., and Ugolini, S. (2008). Functions of natural killer cells. Nat. Immunol. *9*, 503–510.

Wang, J., Li, F., Zheng, M., Sun, R., Wei, H., and Tian, Z. (2012). Lung natural killer cells in mice: phenotype and response to respiratory infection. Immunology *137*, 37–47.

Wenes, M., Shang, M., Di Matteo, M., Goveia, J., Martin-Perez, R., Serneels, J., Prenen, H., Ghesquiere, B., Carmeliet, P., and Mazzone, M. (2016). Macrophage metabolism controls tumor blood vessel morphogenesis and metastasis. Cell Metab. *24*, 701–715.

Xu, C., Fillmore, C.M., Koyama, S., Wu, H., Zhao, Y., Chen, Z., Herter-Sprie, G.S., Akbay, E.A., Tchaicha, J.H., Altabef, A., et al. (2014). Loss of Lkb1 and Pten leads to lung squamous cell carcinoma with elevated PD-L1 expression. Cancer Cell *25*, 590–604.

Xu, D., Han, Q., Hou, Z., Zhang, C., and Zhang, J. (2017). miR-146a negatively regulates NK cell functions via STAT1 signaling. Cell. Mol. Immunol. *14*, 712–720.

Zhang, Q.F., Yin, W.W., Xia, Y., Yi, Y.Y., He, Q.F., Wang, X., Ren, H., and Zhang, D.Z. (2017). Liver-infiltrating CD11b(-)CD27(-) NK subsets account for NK-cell dysfunction in patients with hepatocellular carcinoma and are associated with tumor progression. Cell. Mol. Immunol. *14*, 819–829.

Zhao, E., Maj, T., Kryczek, I., Li, W., Wu, K., Zhao, L., Wei, S., Crespo, J., Wan, S., Vatan, L., et al. (2016). Cancer mediates effector T cell dysfunction by targeting microRNAs and EZH2 via glycolysis restriction. Nat. Immunol. *17*, 95–103.

STAR★METHODS

KEY RESOURCES TABLE

REAGENT or RESOURCE	SOURCE	IDENTIFIER
Antibodies		
Anti-mouse CD107a (1D4B) FITC	BD Biosciences	Cat#553793; RRID: AB_395057
Anti-mouse CD11b (M1/70) APC-CY7	BioLegend	Cat#101226; RRID: AB_830642
Anti-mouse CD11b (M1/70) BV421	BioLegend	Cat#101236; RRID: AB_11203704
Anti-mouse CD11b (M1/70) PerCP-CY5.5	BioLegend	Cat#101228; RRID: AB_893232
Anti-mouse CD122 (TM-β1) FITC	BD Biosciences	Cat#553361; RRID: AB_394808
Anti-mouse CD127 (A7R34) PE	BioLegend	Cat#135010; RRID: AB_1937251
Anti-mouse CD16/32 (2.4G2) PE	BD Biosciences	Cat#553145; RRID: AB_394660
Anti-mouse CD19 (1D3) FITC	BD Biosciences	Cat#557398; RRID: AB_396681
Anti-mouse CD226 (10E5) AF647	BD Biosciences	Cat#565549; RRID: AB_2734133
Anti-mouse CD244 (2B4) PE	BD Biosciences	Cat#553306; RRID: AB_394770
Anti-mouse CD25 (7D4) FITC	BD Biosciences	Cat#553072; RRID: AB_394604
Anti-mouse CD27 (LG.3A10) APC	BioLegend	Cat#124212; RRID: AB_2073425
Anti-mouse CD27 (LG.3A10) BV510	BioLegend	Cat#124229; RRID: AB_2565795
Anti-mouse CD27 (LG.3A10) FITC	BioLegend	Cat#124208; RRID: AB_1236466
Anti-mouse CD27 (LG.3A10) PE	BioLegend	Cat#124210; RRID: AB_1236459
Anti-mouse CD276 (M3.2D7) PE	eBioscience	Cat#12-5973; RRID: AB_466080
Anti-mouse CD3 (145-2C11) APC-CY7	BioLegend	Cat#100330; RRID: AB_1877170
Anti-mouse CD3 (145-2C11) BV510	BioLegend	Cat#100353; RRID: AB_2565879
Anti-mouse CD3 (145-2C11) FITC	BioLegend	Cat#100306; RRID: AB_312671
Anti-mouse CD3 (145-2C11) PerCP-CY5.5	BioLegend	Cat#100328; RRID: AB_893318
Anti-mouse CD4 (GK1.5) PerCP-CY5.5	BioLegend	Cat#100434; RRID: AB_893324
Anti-mouse CD4 (RM4-5) PE	BD Biosciences	Cat#553049; RRID: AB_394585
Anti-mouse CD44 (IM7) PerCP-CY5.5	BD Biosciences	Cat#560570; RRID: AB_1727486
Anti-mouse CD45 (30-F11) BV510	BD Biosciences	Cat#563891; RRID: AB_2734134
Anti-mouse CD45 (30-F11) PE-CY7	BioLegend	Cat#103114; RRID: AB_312979
Anti-mouse CD45.2 (104) APC-CY7	BioLegend	Cat#109824; RRID: AB_830789
Anti-mouse CD49a (Ha31/8) PerCP-CY5.5	BD Biosciences	Cat#564862; RRID: AB_2734135
Anti-mouse CD49b (DX5) APC	BD Biosciences	Cat#560628; RRID: AB_1727502
Anti-mouse CD69 (H1.2F3) FITC	BD Biosciences	Cat#553236; RRID: AB_394725
Anti-mouse CD8 (53-6.7) APC	BioLegend	Cat#100712; RRID: AB_312751
Anti-mouse CD94 (18d3) FITC	eBioscience	Cat#11-0941; RRID: AB_465161
Anti-mouse CD96 (3.3) PE	BioLegend	Cat#131705; RRID: AB_1279389
Anti-mouse CTLA4 (VC10-4F10-11) PE	BD Biosciences	Cat#553720; RRID: AB_395005
Anti-mouse F4/80 (BM8) PerCP-CY5.5	BioLegend	Cat#123128; RRID: AB_893484
Anti-mouse FasL (MFL3) PE	BD Biosciences	Cat#555293; RRID: AB_395711
Anti-mouse FBP1 (EPR4620) Purified	Abcam	Cat#ab109732; RRID: AB_10864942
Anti-mouse Foxp3 (FJK-16s) AF647	eBioscience	Cat#51-5773; RRID: AB_469793
Anti-mouse Gr-1 (RB6-8C5) APC	BioLegend	Cat#108412; RRID: AB_313377
Anti-mouse Granzyme B (16G6) PE	eBioscience	Cat#12-8822; RRID: AB_466216
Anti-mouse IFN-γ (XMG1.2) PerCP-CY5.5	BioLegend	Cat#505822; RRID: AB_961359
Anti-mouse Ki67 (SolA15) AF660	eBioscience	Cat#50-5698-82; RRID: AB_2574235
Anti-mouse LAG3 (C9B7W) APC	BD Biosciences	Cat#562346; RRID: AB_11153127

(*Continued on next page*)

Continued

REAGENT or RESOURCE	SOURCE	IDENTIFIER
Anti-mouse NK1.1 (PK136) PE	BioLegend	Cat#108708; RRID: AB_313395
Anti-mouse NK1.1 (PK136) PE-CY7	BioLegend	Cat#108714; RRID: AB_389364
Anti-mouse NK1.1 (PK136) Purified	BioLegend	Cat#108702; RRID: AB_313389
Anti-mouse NKG2A (16a11) PE	eBioscience	Cat#12-5897; RRID: AB_466026
Anti-mouse NKG2D (CX5) APC	eBioscience	Cat#17-5882; RRID: AB_469464
Anti-mouse NKp46 (29A1.4) AF660	eBioscience	Cat#50-3351; RRID: AB_10598806
Anti-mouse NKp46 (29A1.4) Biotin	BioLegend	Cat#137616; RRID: AB_11218796
Anti-mouse PD-1 (J43) FITC	eBioscience	Cat#11-9985; RRID: AB_465472
Anti-mouse PD-L1 (MIH5) PE	BD Biosciences	Cat#558091; RRID: AB_397018
Anti-mouse Perforin (eBioOMAK-D) APC	eBioscience	Cat#17-9392; RRID: AB_469514
Anti-mouse Tim3 (B8.2C12) APC	BioLegend	Cat#134008; RRID: AB_2562998
Anti-mouse TNF-α (MP6-XT22) PE	BioLegend	Cat#506306; RRID: AB_315427
Anti-mouse TRAIL (N2B2) PE	eBioscience	Cat#12-5951; RRID: AB_466056
Anti-mouse β-Tubulin Purified	Abcam	Cat#ab6046; RRID: AB_2210370
Goat anti-Mouse IgG AF546	Invitrogen	Cat#A-11030; RRID: AB_2534089
Goat anti-Rabbit IgG AF488	Invitrogen	Cat#A-11008; RRID: AB_143165
Goat anti-Rabbit IgG HRP	Boster	Cat#BA1054; RRID: AB_2734136
NK1.1^{+} depletion antibody (PK136)	ATCC	Cat#PK136 (ATCC HB-191)
Chemicals, Peptides, and Recombinant Proteins		
2DG	Sigma	Cat#D8375; CAS: 154-17-6
7AAD	BD Biosciences	Cat#559925
CFSE	Invitrogen	Cat#65-0850-84
Collagenase I	Sigma	Cat#C0130; CAS: 9001-12-1
Glucose	Sigma	Cat#G7528; CAS: 50-99-7
L-Glutamine	Gibco	Cat#25030081
MB05032	MedChemExpress	Cat#HY-16307;CAS:261365-11-1
Oligomycin A	Selleckchem	Cat#S1478; CAS: 579-13-5
Percoll	GE Healthcare	Cat#17089101
Recombinant Human IL-2	Jiangsu Kingsley Pharmaceutical	Cat#S10970056
Recombinant Human TGF-β	PeproTech	Cat#100-21C
Recombinant Mouse IL-12	PeproTech	Cat#210-12
Recombinant Mouse TGF-β	R&D	Cat#7666-MB-005
TRIzol reagent	Invitrogen	Cat#15596018
XF Base Medium Minimal DMEM	Seahorse Bioscience	Cat#102353-100
Critical Commercial Assays		
2×EasyTaq PCR SuperMix	TransGen Biotech	Cat#AS111-13
Anti-Biotin Microbeads	Miltenyi Biotec	Cat#130-090-485
Anti-PE Microbeads	Miltenyi Biotec	Cat#130-048-801
Fluorometric Intracellular ROS Kit	Sigma	Cat#MAK142
Foxp3/Transcription Factor Staining Buffer Set	Invitrogen	Cat#00-5523-00
M-MLV Reverse Transcriptase	Invitrogen	Cat#28025013
Mouse TGF-β1 ELISA kit	Dakewe Biotech	Cat#DKW12-2710
NK Cell Isolation Kit II, mouse	Miltenyi Biotec	Cat#130-096-892
SYBR Premix Ex Taq II	TaKaRa	Cat#RR820
Deposited Data		
Microarray data	This paper	GEO: GSE103856

(*Continued on next page*)

Continued		
REAGENT or RESOURCE	SOURCE	IDENTIFIER
Experimental Models: Cell Lines		
LLC	Shanghai Cell Bank (Chinese Academy of Sciences, Shanghai, China)	Cat# TCM 7
YAC-1	Shanghai Cell Bank (Chinese Academy of Sciences, Shanghai, China)	Cat#TCM28
Oligonucleotides		
Primers for mouse *Il12*, Forward: ACACAGTCCTGGGAAAGTCC; Reverse: TCAGTTTTTCTCTGGCCGTCT	This paper	N/A
Primers for mouse *Tnfα*, Forward: GAACTGGCAGAAGAGGCACT; Reverse: GGTGGTTTGCTACGACGTG	This paper	N/A
Primers for mouse *Mrc1*, Forward: TTTGCCTTTCCCAGTCTCCC; Reverse: CCTCGCGTCCAATAGCTGAA	This paper	N/A
Primers for mouse *Arg1*, Forward: CTACCTGCTGGGAAGGAAGAA; Reverse: TGAGTTCCGAAGCAAGCCAA	This paper	N/A
Primers for mouse *Fbp1*, Forward: GCATCGCACAGCTCTATGGT; Reverse: TTGGATGAGCCATCAAGGGG	This paper	N/A
Primers for mouse *Tgfβ*, Forward: ATGCTAAAGAGGTCACCCGC; Reverse: TGCTTCCCGAATGTCTGACG	This paper	N/A
Primers for mouse *Actin*, Forward: CCACTGTCGAGTCGCGTCC; Reverse: ATTCCCACCATCACACCCTGG	This paper	N/A
Recombinant DNA		
pCDH-CMV-MCS-EF1-copGFP	YouBio	Cat#VT1479
Software and Algorithms		
GraphPad Prism v.5	GraphPad Software	https://www.graphpad.com/
MEV v.4.8.1	Multiple Experiment Viewer	http://mev.tm4.org/

CONTACT FOR REAGENT AND RESOURCE SHARING

Further information and requests for resources and reagents should be directed to and will be fulfilled by the Lead Contact, Haiming Wei (ustcwhm@ustc.edu.cn).

EXPERIMENTAL MODEL AND SUBJECT DETAILS

Mice

Kras^{G12D} (*Kras*) mice were purchased from the Model Animal Research Center of Nanjing University. *Nfil3*$^{-/-}$ mice were kindly provided by Tak Wah Mak from the University of Toronto. *Nfil3*$^{-/-}$ mice were crossed with *Kras* mice to generate *Kras*;*Nfil3*$^{-/-}$ mice. WT mice (without *Kras* mutation) were littermates of *Kras* mice. All mice had a C57BL/6 background and were housed in specific pathogen-free conditions. Mice were maintained under a 12-hour light-dark cycle at 23°C, and had free access to water and standard rodent diet. All experimental procedures involving mice were approved by the ethics committee of the University of Science and Technology of China (Hefei, China).

Cell Lines

Mouse YAC-1 cells (unknown sex) and LLC cells (unknown sex) were purchased from Shanghai Cell Bank (Chinese Academy of Sciences, Shanghai, China). LLC cells were cultured in DMEM (Hyclone) containing 10% FBS (Gibco). YAC-1 were cultured in RPMI-1640 (Hyclone) containing 10% FBS. All cells were maintained at 37°C in a 5% CO_2 incubator.

Plasmids

pCDH-CMV-MCS-EF1-copGFP was used to construct Lenti-Cre by deletion of copGFP, followed by cloning into Cre.

METHOD DETAILS

In Vivo Experiments

In spontaneous models, sex-matched WT, *Kras* and *Kras*;*Nfil3*$^{-/-}$ mice (6–8 weeks) were infected (i.n.) with Lenti-Cre for induction of lung cancer (DuPage et al., 2009). The *Kras* and *Kras*;*Nfil3*$^{-/-}$ mice used in Figures 1I–1K were male, and the other WT and *Kras* mice used in spontaneous models were female. Both female and male mice were used for experiments because no notable sex-dependent differences were found for the reported experiments.

In the LLC model of lung metastasis, LLC cells (8×10^5) in 300 μL of serum-free medium were injected (i.v.) into WT and *Nfil3*$^{-/-}$ mice (male, 6–8 weeks). Mice were sacrificed for tumor, histologic, and immunologic analyses at different time points.

For experiments on NK cell depletion, *Kras* mice were injected (i.v.) weekly with 150 μg of anti-NK1.1 mAb PK136 or IgG (isotype control) in 300 μL of PBS.

For experiments on adoptive transfer of NK cells, LLC cells (8×10^5) in 150 μL of serum-free medium were injected (s.c.) into WT mice (male, 6–8 weeks). Stage 2 lung NK cells were treated with MB05032 (500 μM) or DMSO for 18 h, and were injected into subcutaneous tumors (3×10^5/25μL/mouse) 6 days and 10 days after LLC subcutaneous injection. The tumor volume was calculated as (width^2 × length)/2.

Isolation of Leukocytes, NK Cells, and Macrophages

Lungs from WT and *Kras* mice were cut into pieces and digested in DMEM with collagenase I (1 mg/mL) at 200 rpm/min for 1 h at 37°C, and suspensions were then filtered through sieves. Leukocytes were obtained by suspension in Percoll and centrifugation at 1260 × *g* for 30 min. For isolation of spleen leukocytes, spleens were ground and filtered through sieves. Leukocytes were obtained after lysis of red blood cells.

NK cells (NK1.1$^+$ CD3$^-$) were purified using PE-NK1.1 antibody, anti-PE Microbeads, Biotin-NKp46 antibody, anti-Biotin Microbeads and NK Cell Isolation Kit II. In some experiments (western blotting, RT-PCR, qRT-PCR and microarrays), NK cells were purified by cell sorting (BD Biosciences). Macrophages (F4/80$^+$ Gr-1$^-$) were also purified by cell sorting (BD Biosciences).

Flow Cytometry and Antibodies

After blockade of Fc receptors incubated with rat immunoglobulin for 30 min, leukocytes were stained with fluorescence antibodies for 30 min at 4°C. For CD107a and intracellular staining, leukocytes were incubated with PMA (50 ng/mL; Sigma), ionomycin (1 μg/mL; Sigma), monensin (10 ng/mL; Sigma) and FITC-CD107a for 4 h at 37°C in a 5% CO_2 incubator, followed by staining for extracellular markers. Cells were then fixed, permeabilized with a Foxp3/Transcription Factor Staining Buffer Set and stained for intracellular molecules. The fluorescent antibodies used in this study are shown in Key Resources Table.

Cytokine-Induced Activation of NK Cells

Purified NK cells were stimulated with IL-2 (200 UI/mL) and IL-12 (10 ng/mL) at 37°C in a 5% CO_2 incubator for 18 h. Activation of NK was assessed by detecting levels of CD107a and IFN-γ. In some experiments, MB05032 (500 μM) was added.

TGF-β Stimulation

Purified NK cells were cultured with IL-2 (200 UI/mL), with or without TGF-β (10 ng/mL), at 37°C in a 5% CO2 incubator for 24 h. Cells were then harvested for qPCR.

ELISA

Bronchoalveolar lavage fluid (BALF) was collected by washing the lung once with 1 mL of PBS containing 5 mM of EDTA through a tracheal cannula. BALF was centrifuged, and the supernatants were recovered for measurement of TGF-β levels. The concentration of TGF-β was measured using a Mouse TGF-β1 ELISA kit according to manufacturer instructions.

Viability and Proliferation Assay

Purified NK cells labeled with 5 μM of CFSE were cultured with IL-2 (200 UI/mL) in a 96-well round-bottom plate at 37°C in a 5% CO_2 incubator, with 8×10^4 cells per well. After 120 h, NK cells were harvested and analyzed by FCM. In some experiments, MB05032 (500 μM) and/or 2DG (2 mM) were added.

Cytotoxicity Assay

CFSE-labeled target cells (LLC cells, YAC-1 cells) were co-cultured with purified NK cells with IL-2 (200 UI/mL) at different effector: target ratios (1:1, 4:1, 10:1, 20:1) at 37°C in a 5% CO_2 incubator for 6 h. For the spontaneous death control, CFSE-labeled target cells were cultured alone under the same conditions. Then, 7AAD was added, and lysed cells (CFSE$^+$ 7AAD$^+$) were identified by FCM. In some experiments, MB05032 (500 μM) and/or 2DG (2 mM) were added.

ECAR Analyses

Measurement of the ECAR of NK cells was done using the XF96 Extracellular Flux Analyzer (Seahorse Bioscience). Purified NK cells were stimulated with IL-2 (200 UI/mL) and IL-12 (10 ng/mL) at 37°C in a 5% CO_2 incubator for 18 h. In some experiments, MB05032 (500 μM) was added. Cells were then collected and resuspended in XF Base Medium Minimal DMEM (pH 7.4) with L-Glutamine (2 mM), and were then placed into a cell culture microplate (4 × 10^5 cells per well; XF96; Seahorse Bioscience,). Prior to real-time measurement of the ECAR, glucose (10 mM), oligomycin A (1 μM) and 2DG (50 mM) were added.

ROS Analyses

Purified NK cells were stained using a Fluorometric Intracellular ROS Kit according to manufacturer instructions. The intracellular ROS level was measured by FCM.

Analyses of Gene Expression

Total RNA was isolated using TRIzol reagent, and cDNA synthesis was done using M-MLV Reverse Transcriptase and random primers according to manufacturer instructions. qPCR and PCR were carried out using SYBR Premix Ex Taq and 2×EasyTaq PCR SuperMix, respectively. Primers pairs for target genes are shown in Key Resources Table.

NK cells were isolated from the spleens and lungs for whole-genome transcriptome analyses using SurePrint G3 Mouse Gene Expression (8x60K) microarrays (Agilent Technologies) in duplicate. The heat map of differentially expressed genes was analyzed with MEV v4.8.1. For selecting the differentially expressed genes associated with certain biologic processes, we used the Gene Ontology (GO) project. The microarray data were uploaded to GEO (accession number: GSE103856).

Histology

The left upper lobes of the lungs were placed in 12% neutral buffered formalin overnight, and then dehydrated and embedded in paraffin. Paraffin-embedded tissues were sectioned at 5 μm, followed by hematoxylin and eosin (H&E) staining.

Immunofluorescence

Purified NK cells or frozen sections of lung tumor tissues were fixed with 4% PFA for 15 min, and permeabilized with 0.3% Triton X-100 for 15 min, followed by blockade with 5% goat serum for 1 h at room temperature. Then, sections were incubated with primary antibodies overnight at 4°C. Secondary antibodies were added, followed by staining with DAPI. Stained sections were imaged using a microscope (LSM 710; Zeiss). The antibodies used are shown in Key Resources Table.

Western Blotting

Purified NK cells were lysed in RIPA buffer containing protease inhibitors on ice for 30 min. After centrifugation at 12000 × *g* for 5 min at 4°C, the supernatants were collected for SDS-PAGE. Proteins were then transferred to PVDF membranes, followed by blockade with 5% skimmed milk for 1 h at room temperature. PVDF membranes were incubated with primary antibodies overnight at 4°C, and then incubated with HRP-conjugated secondary antibodies for 1 h at room temperature. Protein bands were developed by chemiluminescence autoradiography. The antibodies used are shown in Key Resources Table.

QUANTIFICATION AND STATISTICAL ANALYSIS

Data are presented as mean ± SEM. Significance between two groups was determined using the two-tailed unpaired *t* test employing the Prism 5 (GraphPad) software. No particular methods were used to determine whether the data met assumptions of the statistical approach. Statistical parameters were represented in the Figure Legend of each Figure. $P < 0.05$ was considered significant. *$p < 0.05$, **$p < 0.01$, and ***$p < 0.001$.

DATA AND SOFTWARE AVAILABILITY

Microarray data have been deposited in GEO: GSE103856.